# Seismic Performance and Evaluation of Controlled Spine Frames Applied in High-rise Buildings

**Xingchen Chen,**[a),b)] **Toru Takeuchi,**[a)] **and Ryota Matsui**[a)]

A controlled spine frame system consists of moment frames and spine frames with concentrated energy-dissipating members. This system guarantees the continuous usability of buildings against Japanese Level-2 earthquake events (similar to DBE events in California), and the authors have confirmed its excellent performance in preventing damage concentration in low-rise buildings. This study further investigates the effect of diverse structural properties on the seismic performance of controlled spine frames applied in high-rise buildings. The effect of building height, yield drift of dampers, spine-to-moment frame stiffness ratio, and damper-to-moment frame stiffness ratio are illustrated in detail, and optimal values are discussed. Also, a segmented spine frame system is proposed for high-rise buildings. The simple evaluation procedure proposed by the authors for low-rise buildings, based on equivalent linearization techniques and response spectrum analyses, was modified to include higher-mode effects for high-rise buildings based on modal analysis. The modified evaluation method was verified by modal pushover and time-history analyses. [DOI: 10.1193/080817EQS157M]

## INTRODUCTION

Damage concentration in limited levels of frame structures has often occurred during major earthquake events, which has raised awareness of the need to improve structural integrity. Various solutions were provided by previous researchers, such as the "strong column–weak beam" concept and the shear wall-frame dual system. Walls usually ensure better structural integrity because of their considerable stiffness. However, they may significantly increase the resisting force and input earthquake energy owing to period shift, and extensive damage may occur at the bottom levels of the shear walls, which is costly and time-consuming to repair. In their study about the effect of foundation flexibility on the seismic performance of a wall-frame system, Paulay and Priestley (1992) found that the loss of wall base restraint would not significantly impair the seismic performance of wall-frame systems. The beneficial spine effect of pin-based walls or columns on the seismic performance of wall-frame systems was verified by studies based on theoretical analyses of multi-degree-of-freedom models or dynamic analyses of building models up to 20 stories (Akiyama et al. 1984, MacRae et al. 2004, Alavi et al. 2004, Tanimura et al. 1996). In recent years, various spine systems with energy-dissipating members were proposed for both new

a) Department of Architecture and Building Engineering, Tokyo Institute of Technology, Tokyo, Japan; Email: xchen@hiroshima-u.ac.jp (XC, corr. author)
b) Current Address: Hiroshima University, Hiroshima, Japan


*Earthquake Spectra*, Volume 34, No. 3, pages 1431–1458, August 2018; © 2018, Earthquake Engineering Research Institute

building applications and retrofitting. Qu et al. (2012) employed a pivoting spine concept in the seismic retrofitting of a concrete building in Japan. Janhunen et al. (2013) proposed a seismic retrofit solution by adding a single pivoting concrete spine to the core of a 14-story building to improve its drift pattern and to distribute yielding at all building levels. Eatherton et al. (2010, 2014) carried out a shake table test of an uplifting steel rocking frame system with post-tensioned (PT) strands to provide self-centering; they also proposed several design concepts for this system. MacRae et al. (2013) studied design considerations for rocking structures. Djojo et al. (2014) proposed a rocking steel panel shear wall with energy dissipation devices. Lai and Mahin (2014) examined the Strongback system, which combines aspects of a traditional concentric braced frame with a stiff mast to prevent damage concentration in a single or a few stories.

However, previous research mainly focused on the first-mode response that dominates building structures, and there are few research results on the seismic performance of high-rise buildings adopting the moment frame with a spine frame dual systems.

A new controlled spine frame was proposed by the authors (Takeuchi et al. 2015, Chen et al. 2017), as shown in Figure 1, and it was applied in the design of a new five-story research center at the Tokyo Tech's Suzukakedai campus. This spine frame consists of (1) a stiff braced steel frame or reinforced concrete (RC) wall (i.e., the spine frame); (2) replaceable energy-dissipating members (herein called buckling restrained columns, or BRCs); and (3) envelope moment-resisting frames. Envelope frames are designed to remain elastic and to control residual drifts, providing self-centering force without resorting to post-tensioning. The input seismic energy is absorbed by the BRCs, which feature significant cumulative deformation capacity and, if required, can easily be replaced following a large earthquake. This combination of structural elements effectively reduces repair costs and downtime of buildings after suffering major earthquakes.

The authors verified the excellent performance of low-rise buildings adopting the proposed spine frame system in preventing damage concentration in weak stories as well as their sufficient self-centering capacity against large earthquake events. The relationship between seismic performance and key structural parameters was studied. A simple yet applicable design method was established with clear limitations and recommendations (Takeuchi et al. 2015, Chen et al. 2017).

However, it was found that the simple controlled spine system is insufficient for high-rise buildings because of higher vibration modes and the larger flexural deformation of the spine

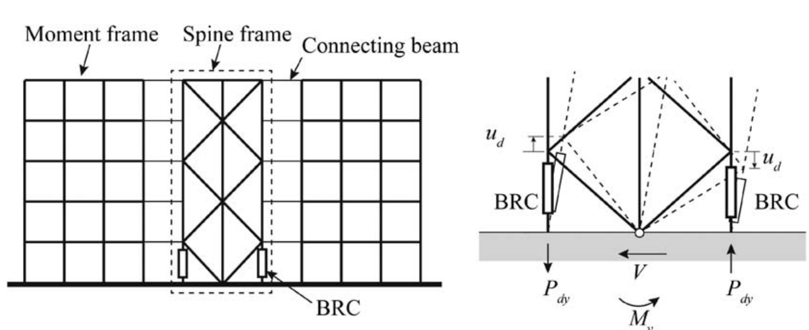


**Figure 1.** Controlled spine frame structure.

frame caused by higher bending moments. Also, the proposed simplified response evaluation method using the assumption of first-mode dominant response showed large errors for higher structures. Here various segmented spine systems are proposed to overcome the limitation of height, and their effects are compared with the simple spine frame. Moreover, two simple response evaluation methods are applied. One is modal pushover analysis; the other is modified response spectrum considering higher vibration modes. The procedures in each method are examined and their validity is confirmed.

## CONTROLLED SPINE FRAMES IN BENCHMARK BUILDINGS

### BENCHMARK BUILDINGS

A parametric study based on a nonlinear time-history analysis was used to investigate the seismic performance of the controlled spine system with diverse structural properties. The benchmark structures used in this study represent typical steel-structure office buildings, as shown in Figure 2a–2c. Besides the continuous single spine (Cnt) model, the corresponding

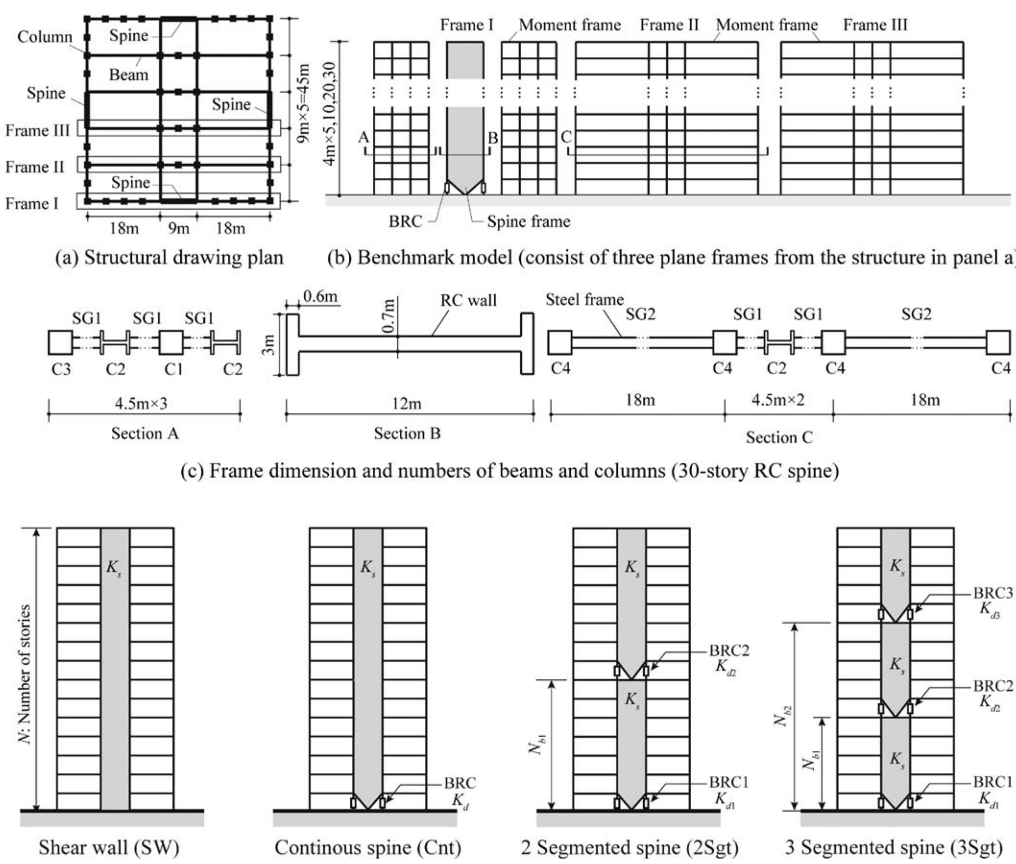


**Figure 2.** Benchmark models of controlled spine frame structures.

shear wall (SW) model was compared with the Cnt model in 5-, 10-, 20-, and 30-story buildings. In order to reduce the base shear of high-rise buildings utilizing the controlled spine frame system, besides the continuous spine, the authors investigated alternative spine configurations, in particular those illustrated in Figure 2d. In segmented spine frame (Sgt) structures, there are two or three spine frames arranged in series along the structure height. All of them are pin-connected at the bottom center to the lower spine or to the foundation structures, and are equipped with BRCs at both edges.

The 2-segment spine (Sgt2) and 3-segment spine (Sgt3) models were compared with the Cnt model in 20- and 30-story buildings, as shown in Figure 2d. The four different-height Cnt structures were designed in elastic ranges as per the base shear ratio (base shear normalized by seismic weight of the structure) of 0.03–0.15. The moment frames and spine frames were assumed to remain elastic during Japanese Level-2 earthquake events (similar to DBE events in California). Although the spine frames can suppress soft story formation, for this study the lateral stiffness of the moment frames was set approximately proportional to the story shear. The spine frames in the 5- and 10-story buildings were assumed to be pin-supported steel trusses, and those in the 20- and 30-story buildings were pin-supported RC walls, to achieve the required stiffness for the parameter studies. The RC walls were assumed to be prestressed by post-tensioning tendons to prevent cracking, and thus stiffness degradation of the RC wall was not considered. The regular member dimensions in each benchmark model are summarized in Table 1.

Member-by-member (MBM) models of the benchmark buildings were built in OpenSees (Mazzoni et al. 2016). Centerline dimension models, which ignore the effects of panel zones and gusset plates, were employed for all models. Beams, columns, and braces or walls were modeled by displacement-based beam elements with elastic materials. P-delta effects were not included. A rigid floor was assumed to ensure that the rocking frame worked with the envelope frame. In the modeling of BRCs, equivalent elastic modulus and equivalent strain hardening ratio were adopted in order to consider the contribution of the higher axial stiffness of the elastic portions of the same member. The BRC material was assumed to have bilinear stress-strain relations with a kinematic hardening rule. Rayleigh damping with a 0.02 critical damping ratio matching at the first and third modes was implemented in the model.

## PARAMETERIZING KEY STRUCTURAL PROPERTIES

The key structural properties, considered highly related to the seismic performance of spine frame structures, were the stiffness of the moment frames, spine frames, and dampers. The stiffness of the moment frame, denoted $K_f$, is given as:

$$K_f = \frac{12}{h^2 \sum_{n=1}^{N} \left( \frac{1}{(EI/h)_{cn}} + \frac{1}{(EI/l)_{bn}} \right)} \tag{1}$$

where $h$ represents the story height and $(EI/h)_{cn}$ and $(EI/l)_{bn}$ are the sums of line stiffness of all columns and beams at the $n$th story, respectively. $N$ is the total number of stories.

**Table 1.** Dimensions of beams and columns in the moment frame (mm)

| Model | C1 | C2 | C3 | C4 | SG1 | SG2 |
|---|---|---|---|---|---|---|
| 5-story | □-500 × 19–22 | H-500 × 350 × 25 × 28–32 | □-500 × 19–22 | □–600 × 32 | H-600 × 300 × 12 × 22–25 | H-1000 × 300 × 19 × 32 |
| 10-story | □-600 × 19–28 | H-650 × 400 × 16 × 22–28 | □-600 × 19–25 | □–650 × 28–32 | H-650 × 300 × 16 × 25–32 | H-900 × 300 × 19 × 25 |
| 20-story | □-600 × 19–28 | H-650 × 400 × 16 × 22–28 | □-600 × 19–25 | □–650 × 28–32 | H-700 × 300 × 16 × 22–30 | H-900 × 300 × 19 × 25 |
| 30-story | □-700 × 19–28 | H-750 × 500 × 16 × 22–28 | □-700 × 19–25 | □–750 × 28–32 | H-750 × 300 × 16 × 22–32 | H-1000 × 300 × 19 × 25 |

The lateral stiffness of the spine frame, denoted $K_s$, is defined considering both bending and shear stiffness:

$$K_{sb} = \frac{3(EI)_s}{H^3}, \quad K_{ss} = \frac{(GA)_s}{H}, \quad K_s = \frac{1}{\frac{1}{K_{ss}} + \frac{1}{K_{sb}}} \tag{2}$$

where $(EI)_s$ is the equivalent sectional bending stiffness of the spine frame; $(GA)_s$ is the equivalent sectional shear stiffness of the spine frame; $H$ is the total height of the structure, which is identical to the height of the spine frame; and $K_{sb}$ and $K_{ss}$ are the equivalent bending stiffness and shear stiffness of the spine frame, respectively. The lateral stiffness of the dampers, denoted $K_d$, is calculated as:

$$K_d = \frac{F_{BRC\_y}(b)^2}{2u_{BRC\_y}(H_{eq})^2} \tag{3}$$

where $u_{BRC\_y}$ is the yield deformation of each BRC; $b$ is the width of the spine frame; $F_{BRC\_y}$ represents the yielding force of the BRC; and $H_{eq}$ is the equivalent height of the first mode. Values of the representative stiffnesses of the benchmark buildings are summarized in Table 2. The representative stiffness was further parameterized into normalized stiffness ratios, (i.e., the stiffness ratio of spine frame to moment frames), denoted $K_s/K_f$, and the stiffness ratio of dampers to moment frames, denoted $K_d/K_f$. They were used as the control parameters in the parametric study. In the benchmark models, $\theta_y = 0.1\%$, $K_d/K_f = 1.0$, and $K_s/K_f = 0.5$ in the 5- and 10-story buildings, while $K_s/K_f = 0.3$ in the 20- and 30-story buildings. Considering the seismic design code and construction requirements, in the parametric study $K_d/K_f$ ranged from 0.5 to 4.0, and $K_s/K_f$ ranged from 0.1 to 2.0. Table 3 summarizes the variables of the four buildings. A total of 564 cases were studied.

## INPUT GROUND MOTIONS IN TIME-HISTORY ANALYSES

A time-history analysis was carried out to examine seismic performance. The ground motions used included the artificial wave BCJ-L2 with duration of 120 s, as well as the observed waves of El Centro NS (1940), JMA Kobe NS (1995), TAFT EW (1925), and Hachinohe NS (1968), each 30 s long. The acceleration response spectra of the four recorded

**Table 2.** Structural properties of spine frame, BRC hinge[a] and representative stiffnesses

| | Spine frame | | BRC hinge | | Representative stiffness | | |
|---|---|---|---|---|---|---|---|
| Model | $EI$ (kNm$^2$) | $GA$ (kN) | $M_y$ (kNm) | $\theta_y$ (rad) | $K_f$ (kN/m) | $K_s$ (kN/m) | $K_d$ (kN/m) |
| 5-story | $2.9 \times 10^8$ | $4.0 \times 10^6$ | $3.0 \times 10^4$ | 0.10% | $1.4 \times 10^5$ | $7.0 \times 10^4$ | $1.4 \times 10^5$ |
| 10-story | $9.1 \times 10^8$ | $1.2 \times 10^7$ | $6.4 \times 10^4$ | 0.10% | $7.5 \times 10^4$ | $3.8 \times 10^4$ | $7.5 \times 10^4$ |
| 20-story | $2.0 \times 10^9$ | $1.4 \times 10^8$ | $1.3 \times 10^5$ | 0.10% | $3.9 \times 10^4$ | $1.2 \times 10^4$ | $3.9 \times 10^4$ |
| 30-story | $6.0 \times 10^9$ | $2.1 \times 10^8$ | $2.6 \times 10^5$ | 0.10% | $3.5 \times 10^4$ | $1.0 \times 10^4$ | $3.5 \times 10^4$ |

[a] The BRC hinge represents a pair of BRCs at the bottom or segment level of the spine frame: $M_y = F_{BRC\_y} \cdot b$, $\theta_y = 2u_{BRC\_y}/b$, where $F_{BRC\_y}$ and $u_{BRC\_y}$ are the axial yielding force and deformation of a BRC, respectively and $b$ is the lateral distance between a pair of BRCs.

**Table 3.** Variables in the parametric study

**Sgt3**-**Ksf**0.3-**Nb**10-20-**Kdf**1.0-1.0-1.0
① ② ③ ④

① Model type
**SW**: Shear wall **Cnt**: Continous spine
**Sgt2**: 2 Segmented spines **Sgt3**: 3 Segmented spines

② Stiffness ratio of the spine and the moment frame
**Ksf** $K_s/K_f$

③ Stories of the upper BRCs
(excluded in SW or Cnt model)
Sgt2: **Nb** $N_{b1}$
Sgt3: **Nb** $N_{b1}$-$N_{b2}$

④ Stiffness ratio of the dampers and
the moment frame (excluded in SW model)
Cnt: **Kdf** $K_d/K_f$
Sgt2: **Kdf** $K_{d1}/K_f$-$K_{d2}/K_f$
Sgt3: **Kdf** $K_{d1}/K_f$-$K_{d2}/K_f$-$K_{d3}/K_f$

| | | | | | | | | | | |
|---|---|---|---|---|---|---|---|---|---|---|
| All | $K_s/K_f$ | 0.1 | 0.3 | 0.5 | 0.7 | 1 | 2 | | | |
| Cnt | $K_d/K_f$ | 0 | 0.5 | 0.8 | 1 | 1.3 | 1.5 | 2 | 3 | 4 |
| Sgt2 | $N_{b1}$ | 3~29 | | | | | | | | |
| | $K_{d1}/K_f$ | 0 | 0.5 | 0.8 | 1 | 1.3 | 1.5 | | | |
| | $K_{d2}/K_{d1}$ | 0.5 | 0.8 | 1 | | | | | | |
| Sgt3 | $N_{b1}$ | 10~20 | | | | | | | | |
| | $N_{b2}$ | 14~28 | | | | | | | | |
| | $K_{d1(2,3)}/K_f$ | 1 | | | | | | | | |

ground motions were spectrally matched to follow the Japanese life safety design spectrum (BRI-L2), as shown in Figure 3.

## SEISMIC EVALUATION BASED ON MODAL PUSHOVER ANALYSIS

### EVALUATION PROCEDURE

Besides the evaluations by time-history analyses using MBM models, two simplified response evaluation methods using the key parameters were proposed. The modal pushover analysis (MPA) based on the structural dynamics theory has been commonly used for seismic evaluation (Krawinkler et al. 1998). In a typical MPA procedure, a suit of monotonically increasing lateral forces with an invariant heightwise distribution is loaded on the structure until a target deformation is reached (Chopra et al. 2002). Both force distribution and target deformation are calculated by assuming that one mode response is predominant and the mode shape remains unchanged after the yielding mechanism occurs. The invariant force distribution cannot consider the redistribution of inertia forces after the yielding mechanism occurs,

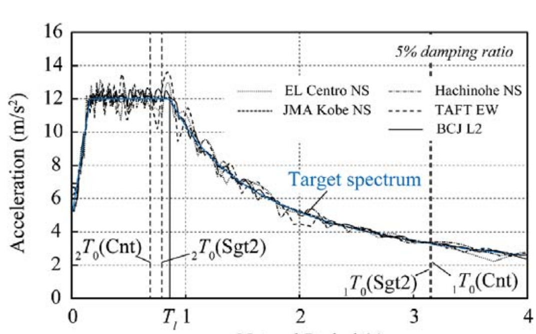


**Figure 3.** Acceleration spectra of normalized input ground motions.

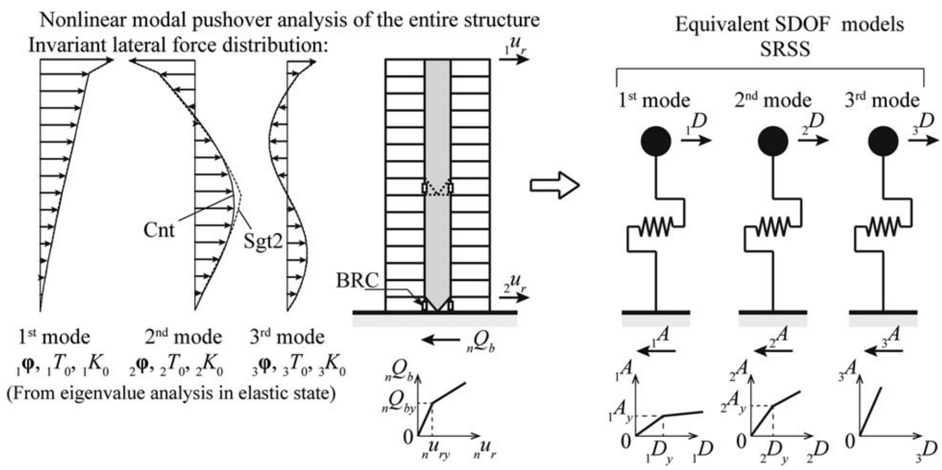


**Figure 4.** Nonlinear modal pushover analysis for spine frame structures.

but they are conceptually and computationally simple for engineering practice. In the current study, a MPA procedure with invariant force distribution considering the contribution of higher modes was used for evaluating the proposed continuous and segmented spine frame structures applied in high-rise buildings, as shown in Figure 4.

Chopra et al. proposed a modified MPA procedure assuming the higher modes as elastic, and verified its accuracy for regular frames (Chopra et al. 2004). However, this assumption significantly overestimates seismic performance, particularly the force response of spine frames in controlled spine frame structures. Therefore, a nonlinear pushover analysis is required for higher modes, at least for the second mode of spine frame structures.

The evaluation procedure was as follows:

In Step 1, compute the natural periods, ${}_nT_0$, and modes, ${}_n\boldsymbol{\varphi}$, for a linearly elastic vibration of the building.

In Step 2, for the $n$th mode, develop the base shear-floor displacement, ${}_nQ_b$-${}_nu_r$ pushover curve by nonlinear static analysis of the building using the lateral force distribution, ${}_n\mathbf{q}*$ (Equation 4; $\mathbf{m}$ is mass matrix).

$$ {}_n\mathbf{q}* = \mathbf{m}_n\boldsymbol{\varphi} \tag{4} $$

In Step 3, convert the ${}_nQ_b$-${}_nu_r$ pushover curve to the force-deformation, ${}_nA$-${}_nD$, relation for the $n$th mode inelastic SDOF system using Equation 5 (${}_nM_{eq}$ is the effective modal mass; ${}_n\beta$ is a modal participation factor; ${}_nu_r$ is reference floor displacement; and ${}_nQ_b$ is base shear force). The section *Reference Floor* explains how to determine the reference floor.

$$ {}_nA = \frac{{}_nQ_b}{{}_nM_{eq}} \quad {}_nD = \frac{{}_nu_r}{{}_n\beta_n\varphi_r}, \quad {}_n\beta = \frac{{}_n\boldsymbol{\varphi}^T\mathbf{m}\{1\}}{{}_n\boldsymbol{\varphi}^T\mathbf{m}_n\boldsymbol{\varphi}}, \quad {}_nM_{eq} = \frac{({}_n\boldsymbol{\varphi}^T\mathbf{m}\{1\})^2}{{}_n\boldsymbol{\varphi}^T\mathbf{m}_n\boldsymbol{\varphi}} \tag{5} $$

In Step 4, from the ${}_nA$-${}_nD$ relation, determine the initial stiffness and hardening stiffness of the SDOF system.

In Step 5, evaluate the peak deformation, ${}_nD$, using Equations 6–9 iteratively.

$$ {}_nh_{eq} = {}_nh_0 + \frac{2}{\pi\mu p}\ln\frac{(1-p+p\mu)}{(\mu)^p} \tag{6} $$

$$ {}_nT_{eq} = {}_nT_0\sqrt{\frac{\mu}{1+p(\mu-1)}} \tag{7} $$

where $p = \frac{{}_nK_h}{{}_nK_0}$ denotes the hardening stiffness ratio; and $\mu = \frac{{}_nD_t}{{}_nD_y}$ denotes the ductility ratio when the target deformation is assumed as ${}_nD_t$; ${}_nD_y$ is the yielding deformation; and ${}_nD_0$ and ${}_nA_0$ denote the primarily estimated deformation and force corresponding to the initial period, ${}_nT_0$, and initial damping ratio, ${}_nh_0$ (=0.02), respectively. They are updated by Equations 8 and 9 until a convergence is reached, where ${}_nR_d$ and ${}_nR_a$ are the deformation and force reduction factors:

$$ {}_nD = {}_nR_{dn}D_0,\ {}_nR_d = \begin{cases} \frac{{}_nT_{eq}}{{}_nT_0}{}_nD_h & T_l \le {}_nT_0 \le {}_nT_{eq} \\ \frac{{}_nT_{eq}}{{}_nT_0}{}_nD_h\frac{T_l(2{}_nT_{eq}-{}_nT_l)-({}_nT_0)^2}{2({}_nT_{eq}-{}_nT_0){}_nT_0} & {}_nT_0 \le T \le {}_nT_{eq}, \quad T_l = 0.864\text{ s} \\ \frac{{}_nT_{eq}}{{}_nT_0}{}_nD_h\frac{{}_nT_{eq}+{}_nT_0}{2{}_nT_0} & {}_nT_0 \le {}_nT_{eq} \le T_l \end{cases} \tag{8} $$

${}_nD_h = \sqrt{\frac{1+\alpha_n h_0}{1+\alpha_n h_{eq}}}$, $\alpha$ is an empirical value, set as 25.

$$ {}_nA = {}_nR_{an}A_0,\ {}_nR_a = {}_nR_d\left(\frac{{}_nT_f}{{}_nT_{eq}}\right)^2 \tag{9} $$

In Step 6, inversely convert ${}_nD$ to the peak $i$th floor displacement, ${}_nu_i$, in the inelastic MDOF system.

In Step 7, from the pushover database (Step 2), extract values of desired response, ${}_nr$, at the $i$th floor displacement equal to ${}_nu_i$.

In Step 8, repeat Steps 3–7 for as many modes as required for sufficient accuracy.

In Step 9, determine the total seismic response by combining the peak modal responses using a modal combination rule.

The MPA procedure can also be used to estimate internal forces in those structural members that remain within their linearly elastic range, but not in those that deform into the inelastic range. In the latter case, the member forces are estimated from the total member deformations.

## REFERENCE FLOOR

The assumption of invariable mode shapes before and after the yielding mechanism occurs might not be satisfied, particularly for spine frame structures, because the yielding deformation concentrates in dampers that are equipped at specific stories. Therefore,

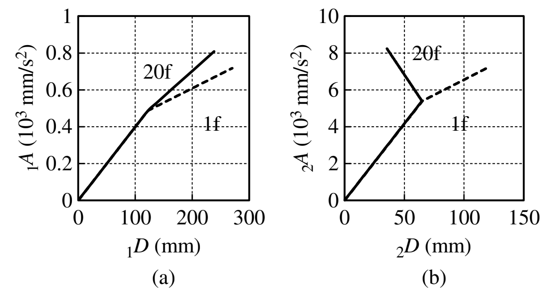


**Figure 5.** SDOF force-deformation (A-D) curves obtained using 1st or 20th floor as reference floor (model: 20-story Cnt-Ksf0.3-Kdf1.0; input: BCJ-L2). (a) A-D curves of first mode vibration and (b) A-D curves of second mode vibration.

the relationship between the different floor displacements and base shears obtained from the pushover analysis of the original structure resulted in a different hardening stiffness ratio (even reversal deformation) in the force-deformation curve of the corresponding SDOF system, as shown in Figure 5a.

Previous researchers also observed "reversal" curves in the higher-mode pushover analysis and suggested using lower floors as reference floors (Chopra et al. 2005). For spine frame structures, the estimation of responses using the SDOF was more conservative when the hardening stiffness ratio was larger. For the first mode, the top floor gave the largest hardening stiffness ratio; for the second mode, the first floor gave almost the largest hardening stiffness ratio (Figure 6). Similar results were obtained for the Sgt2 models. These two floors were determined to be the reference floors for first and second modes, respectively.

## SEISMIC EVALUATION BASED ON RESPONSE SPECTRUM ANALYSIS

### EVALUATION PROCEDURE

Chen et al (2017) proposed a simplified evaluation method based on equivalent linearization techniques and response spectrum analysis (RSA) for low-rise spine frame structures. It was

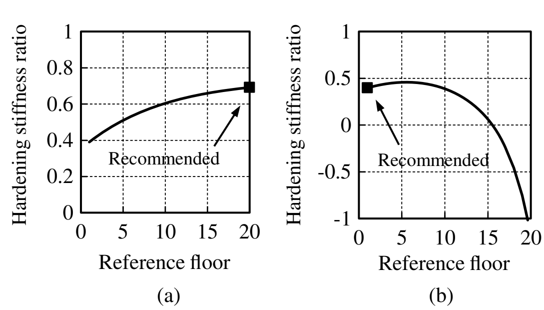


**Figure 6.** Hardening stiffness ratio obtained using different reference floors (model: 20-story Cnt-Ksf0.3-Kdf1.0; input: BCJ-L2). (a) Hardening stiffness ratio of first mode vibration and (b) Hardening stiffness ratio of second mode vibration.

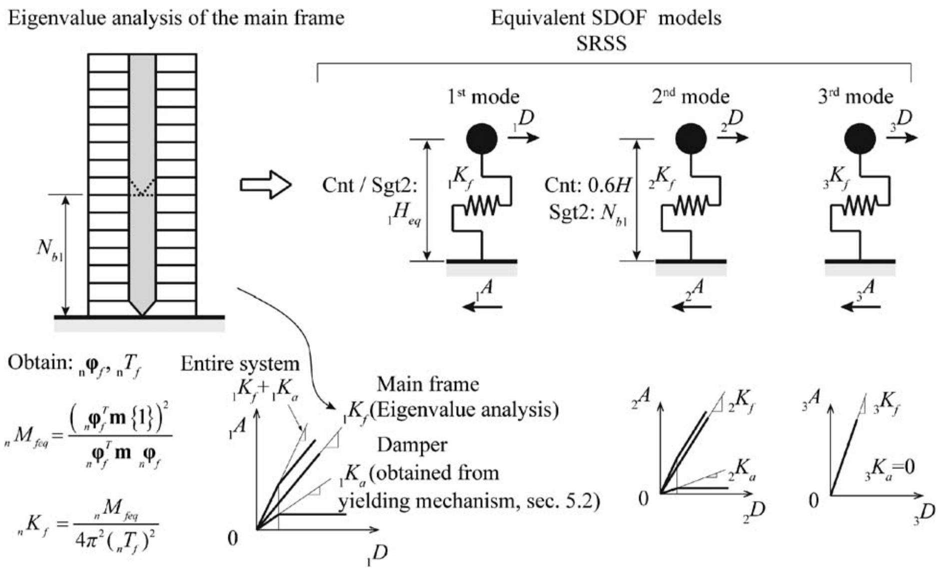


**Figure 7.** Multimode response spectrum analysis for spine frame structures.

verified that this method provides enough accuracy when the key structural parameters are in a regular range, which Chen et al. quantified. Here, the modified procedure including the higher-mode contribution to the seismic performance of high-rise buildings (Figure 7) is proposed.

In Step 1, compute the natural periods, ${}_nT_f$, and modes, ${}_n\boldsymbol{\varphi}_f$, for the linearly elastic vibration of the main frame without BRCs. Obtain the elastic force-deformation relation, ${}_nA$-${}_nD$, with stiffness, ${}_nK_f$, for the SDOF system using Equation 5.

In Step 2, evaluate the elastic modal responses, ${}_nr_f$, of the main frame with an inherent damping ratio of 0.02. To evaluate the forces of the structural members, an elastic pushover analysis using the lateral force distribution, ${}_n\mathbf{q}_f*$, is required (${}_n\mathbf{q}_f* = \mathbf{m}_n\boldsymbol{\varphi}_f$).

In Step 3, for the $n$th mode, compute the additional stiffness, ${}_nK_a$, and yielding deformation, ${}_nD_y$, contributed by the BRCs. Determine the system initial stiffness, ${}_nK_{f+a} = {}_nK_f + {}_nK_a$. The system hardening stiffness equals ${}_nK_f$ obtained from Step 1.

In Step 4, compute the deformation and force reduction factors, ${}_nR_d$ and ${}_nR_a$, using Equations 6–9 iteratively, where ${}_nK_0$ and ${}_nK_\mathrm{h}$ are replaced with ${}_nK_{f+a}$ and ${}_nK_f$. Equation 8 is replaced with Equation 10 because the main frame herein excludes the dampers (${}_nT_{f+a}$ in RSA equals ${}_nT_0$ in MPA; both are the initial stiffness of the whole system):

$$
{}_nR_d \begin{cases} \frac{{}_nT_{eq}}{{}_nT_f}\,{}_nD_h & T_l \le {}_nT_{f+a} \le {}_nT_{eq} \le {}_nT_f \\ \frac{{}_nT_{eq}}{{}_nT_f}\,{}_nD_h\,\frac{T_l(2{}_nT_{eq}-{}_nT_l)-{}_nT_{f+a}^2}{2({}_nT_{eq}-{}_nT_{f+a})T_l} & {}_nT_{f+a} \le T_l \le {}_nT_{eq} \le {}_nT_f \\ \frac{{}_nT_{eq}}{{}_nT_f}\,{}_nD_h\,\frac{{}_nT_{eq}+{}_nT_{f+a}}{2T_l} & {}_nT_{f+a} \le {}_nT_{eq} \le T_l \le {}_nT_f \\ \frac{{}_nT_{eq}}{{}_nT_f}\,{}_nD_h\,\frac{{}_nT_{eq}+{}_nT_{f+a}}{2{}_nT_f} & {}_nT_{f+a} \le {}_nT_{eq} \le {}_nT_f \le T_l \end{cases} \tag{10}
$$

In Step 5, evaluate the desired responses of the original structure by multiplying ${}_nR_d$ or ${}_nR_a$.

In Step 6, repeat Steps 3–5 for as many modes as required for sufficient accuracy.

In Step 7, determine total seismic response by combining peak modal responses using the SRSS modal combination rule.

Note that in the RSA procedure, the static pushover analysis is not necessary for evaluating the maximum deformation and story shear of the entire structure, unless the results of structural member-level forces are desired. The effect of damper stiffness can be simply estimated by formula calculation without numerical analysis, which is more convenient than MPA.

## ESTIMATION OF DAMPER STIFFNESS

Generally, connection elements have a significant influence on the effectiveness of damping devices, reducing the imposed local deformations and achieved damping for a given level of drift. For controlled spine frame structures, spine frame flexural stiffness reduces effective damper stiffness and must be accounted for. To isolate spine frame stiffness in the member-by-member model, an eigenvalue analysis was first conducted with the dampers substituted with rigid elements (Figure 8a) and then with the dampers removed (Figure 8b). Thus, the stiffness of the spine frame $K_c$ could be isolated from the frame $K_f$ by subtracting the results of the first pushover analysis $(K_c + K_f)$ from the second $K_f$. The local damper stiffness $K_d$ was determined as described in the following sections. Finally, the stiffness of the entire structure is expressed by Equation 11:

$$K_a = \frac{1}{\frac{1}{K_d} + \frac{1}{K_R - K_f}} \tag{11}$$

### Damper Stiffness and Yielding Deformation of Cnt Models

The estimation of damper stiffness is essential for ensuring the accuracy of the RSA results because the stiffness of the main frame, $K_f$, is obtained directly from the eigenvalue analysis, which is regarded as accurate. Damper stiffness and yielding deformation in the

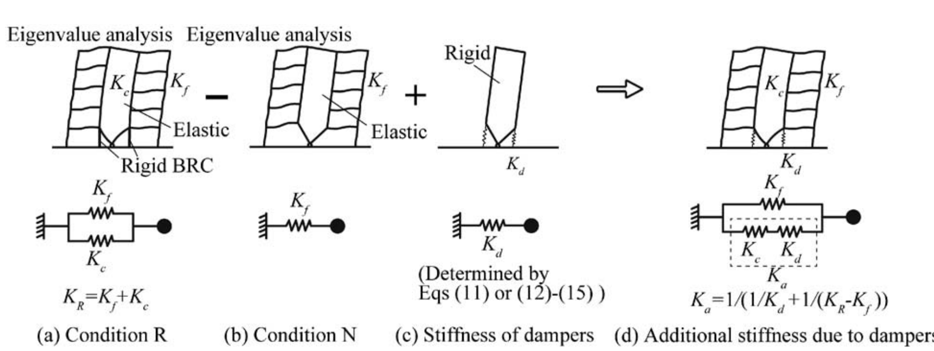


**Figure 8.** Computation of additional stiffness considering flexural deformation of spine frames.

first- or second-mode SDOF system of the Cnt models is calculated using Equation 12a and 12b. The damper stiffness in modes higher than the second mode can be ignored because the generated error in total response is usually less than 0.1% for spine frame structures.

$$ {}_iK_d = \frac{F_{BRC\_y}(b)^2}{2u_{BRC\_y}({}_iH_d)^2} \cdot \frac{1}{{}_iM_{eq}}, \quad i = 1, 2 \tag{12a} $$

$$ {}_iD_{dy} = \frac{2u_{BRC\_y}}{b_i\beta_i\varphi_1/h_1} \cdot \frac{{}_iK_a}{{}_iK_d}, \quad i = 1, 2 \tag{12b} $$

where ${}_iH_d$ is the height of the equivalent damping force location (${}_1H_d = {}_1H_{eq}$ for the first mode; ${}_2H_d = 0.6H$ for the second mode); ${}_iK_d$ is the damper stiffness in the first-mode ($i = 1$) or second-mode ($i = 2$) of the SDOF system; $F_{BRC\_y}$ and $u_{BRC\_y}$ are the yielding axial force and yielding deformation of a single BRC, respectively; $b$ is the lateral distance between a pair of BRCs; and $h_1$ is the height of the first story.

The equivalent force represents a concentrated horizontal force possessing the same value with shear force allocated by the additional damper system; it can generate an identical overturning moment as the distributed horizontal forces. The elastic modal stiffness obtained by MPA is used to calculate ${}_iH_d$ for the first- and second-mode SDOF systems in RSA in order to validate Equation 12. Figure 9 shows that ${}_1H_d$ is almost identical to ${}_1H_{eq}$ and the effects of $K_s/K_f$ and $K_d/K_f$ on both are negligible. Initial stiffness, yielding deformation, and maximum deformation evaluated using RSA and MPA are almost identical (Appendix A, Figure A1).

There is a slight increase in ${}_2H_d/H$ with $K_s/K_f$; it reaches 0.6 when $K_s/K_f = 2.0$. Although it is assumed that ${}_2H_d = 0.6H$ causes a larger error when $K_s/K_f$ is smaller, such difference has little effect on the initial stiffness or yielding deformation of the second-mode vibration of the system (Appendix A, Figure A2), because main frame stiffness rather than the damper stiffness is dominant in the second-mode stiffness.

Since main frame stiffness is accurate in RSA, we can use it to validate the main frame stiffness obtained by MPA. Figure 10 compares the detailed A-D curves of a Cnt model obtained by RSA and MPA. These A-D curves march well in the first mode vibration, and the initial stiffness of the second mode vibration obtained by the two methods are in

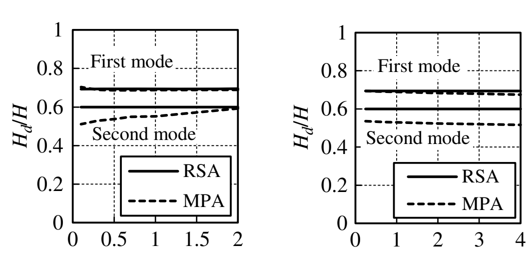


(a) $H_d/H$ with various $K_s/K_f(K_d/K_f$=1.0)

(b) $H_d/H$ with various $K_d/K_f(K_s/K_f$=0.3)

**Figure 9.** Verification of $H_d$ for Cnt models by MPA.

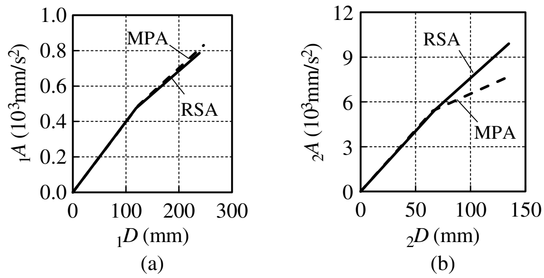


**Figure 10.** Comparison of RSA and MPA in SDOF A-D curves of Cnt models (model: 20-story Cnt-Ksf0.3-Kdf1.0). (a) A-D curves of first mode vibration and (b) A-D curves of second mode vibration.

good agreement. However, we can see that in the second mode vibration, the hardening stiffness (i.e., the stiffness of the main frame, obtained by the eigenvalue analysis in RSA) is much larger than the MPA result, mainly because the lateral force distribution used in MPA is kept proportional to the elastic force distribution and underestimates the post-yield stiffness. Comparison of the hardening stiffness of other Cnt models can be found in Appendix A, Figures A1 and A2.

### Damper Stiffness and Yielding Deformation of Sgt Models

Calculation of damper stiffness, ${}_iK_d$, for the Sgt2 models is relatively more complicated than for the Cnt models. As for the first mode, the elastic deformations of both BRC1s and BRC2s are taken into account (Equations 13–15). It is assumed that ${}_1H_{eq}$ is the location of the equivalent concentration force. As for the second mode, the BRC2s are assumed to yield initially because the MPA results show that they make little contribution to overall damper stiffness (Equation 16). Detailed explanation of the yielding mechanism of dampers in the Sgt2 models is found in Appendix B. The height of the BRC2s, $H_{Nb}$, is assumed as the location of the equivalent concentration force, as shown in Figure 11. Yielding deformations are calculated in Equation 12b. Figure 12shows that ${}_1H_{eq}$ and $H_{Nb}$ match well with the height obtained from MPA.

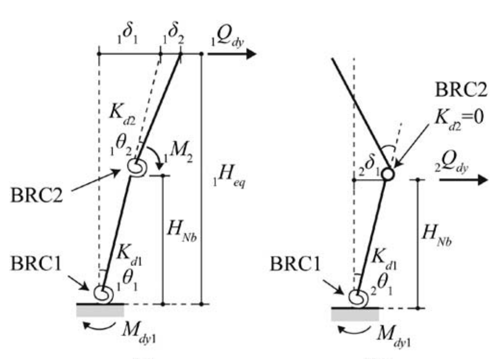


**Figure 11.** Computation of damper stiffness of a Sgt2 model. (a) Equivalent mechanical model for first mode vibration and (b) equivalent mechanical model for second mode vibration.

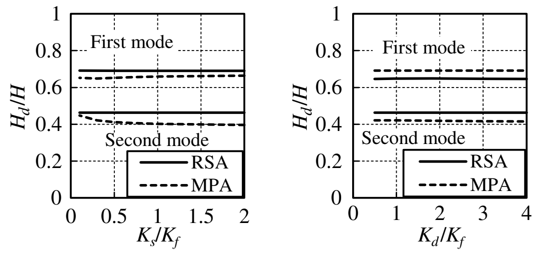


(a) $H_d/H$ with various $K_s/K_f(K_d/K_f=1.0)$

(b) $H_d/H$ with various $K_d/K_f(K_s/K_f=0.3)$

**Figure 12.** Verification of $H_d$ for Sgt2 models by MPA.

$$\begin{cases} {}_1\theta_2 = {}_1M_2/K_{d2} \\ {}_1M_2 = {}_1Q_{dy}({}_1H_{eq} - H_{Nb}) \rightarrow {}_1\delta_2 = \frac{{}_1Q_{dy}({}_1H_{eq}-H_{Nb})^2}{K_{d2}} \\ {}_1\delta_2 = {}_1\theta_2({}_1H_{eq} - H_{Nb}) \end{cases} \tag{13}$$

$$\begin{cases} {}_1\theta_1 = M_{dy1}/K_{d1} \\ M_{dy1} = {}_1Q_{dy1}H_{eq} \rightarrow {}_1\delta_1 = \frac{{}_1Q_{dy1}H_{eq}^2}{K_{d1}} \\ {}_1\delta_1 = {}_1\theta_1 \cdot {}_1H_{eq} \end{cases} \tag{14}$$

$$ {}_1K_d = \frac{{}_1Q_{dy}}{({}_1\delta_1 + {}_1\delta_2){}_1M_{eq}} = \frac{1}{\frac{{}_1H_{eq}^2}{K_{d1}} + \frac{({}_1H_{eq}-H_{Nb})^2}{K_{d2}}} \cdot \frac{1}{{}_1M_{eq}} \tag{15}$$

$$ {}_2K_d = \frac{M_{dy1}}{\theta_{dy1}(H_{Nb})^2{}_2M_{eq}} = \frac{K_{d1}}{(H_{Nb})^2{}_2M_{eq}} \tag{16}$$

where $K_{d1}$ and $K_{d2}$ are the rotational stiffnesses of the elastoplastic hinges formed by the BRC1s and BRC2s; $M_{dy1}$ is the yielding moment of hinge BRC1; ${}_1Q_{dy}$ is the lateral force at a height of ${}_1H_{eq}$ when hinge BRC1 yields in the first-mode SDOF system; and ${}_1M_2$ is the elastic moment of hinge BRC2 when subjected to the lateral force, ${}_1Q_{dy}$, in the first-mode SDOF system.

Generally, the initial stiffness and yielding deformation of the first- and second-mode SDOF systems determined by RSA are in good agreement with those determined by MPA when $K_s/K_f = 0.0 - 2.0$ and $K_{d1}/K_f = 0.0 - 2.0$ (Figure 13; Appendix A, Figures A3 and A4a-1, A4a-2, A4b-1, and A4b-2). The second-mode hardening stiffness of RSA is much larger than that of MPA. As with the Cnt models, the main reason is that the lateral force distribution used in MPA is kept proportional to the elastic force distribution, and it underestimates the post-yield stiffness. As a result, the difference between RSA and MPA in hardening stiffness increases as $K_{d1}/K_f$ increases (Appendix A, Figures A3, A4a-3, and A4b-3).

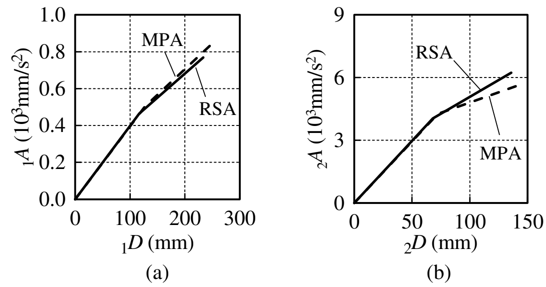


**Figure 13.** Comparison of RSA and MPA in SDOF A-D curves of Sgt2 models (model: 20-story Sgt2-Ksf0.3-Kdf1.0-0.5). (a) A-D curves of first mode vibration and (b) A-D curves of second mode vibration.

## PARAMETRIC STUDY OF EACH CONTROLLED SPINE SYSTEM USING TIME-HISTORY ANALYSIS

### SEISMIC BEHAVIOR OF CNT MODELS

In this section, the response characteristics of each spine system proposed in Figure 2 are compared and discussed using the parameters $K_d$, $K_f$, and $K_s$ as defined in previous sections. The averaged results for story drift ratio (SDR), story shear ratio (story shear normalized by structure seismic weight) obtained by time-history analysis with various inputs are summarized in Figure 14 along with the first-mode natural period of the SW and Cnt models.

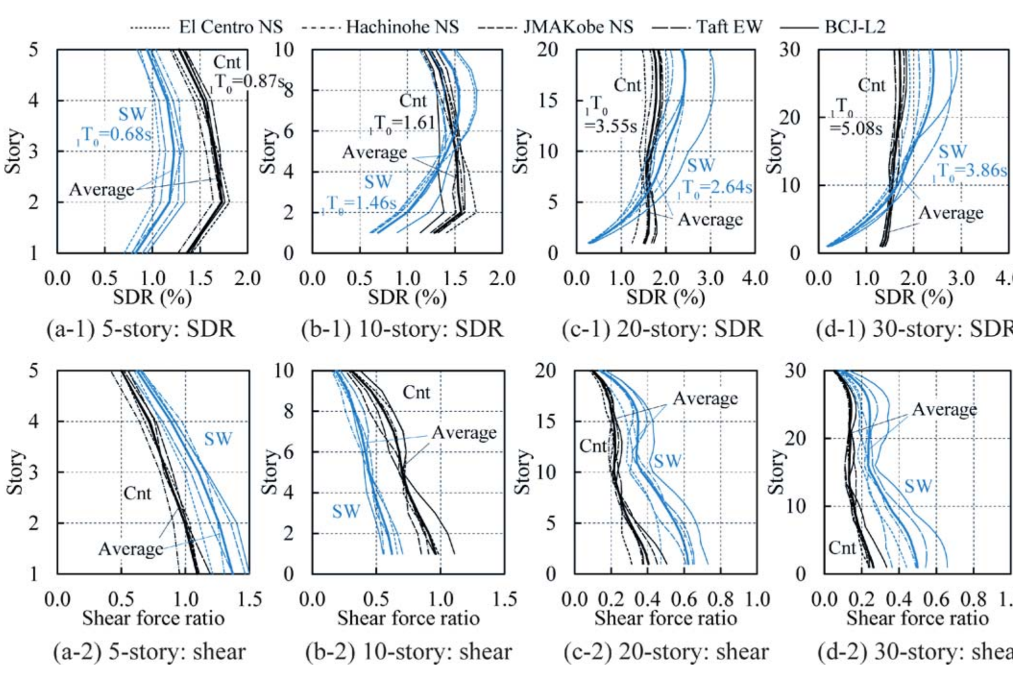


**Figure 14.** Seismic performance of Cnt and SW models with various heights.

The higher mode effect is observed in the shear force distribution of the 20- to 30-story buildings. Except for the SDR of the 5-story building, both the SDR and the shear force response in the controlled Cnt models are smaller than in the SW models. The main reason for this is the shift period of the softer Cnt models, particularly for the taller buildings. The SDR of the Cnt models is more uniformly distributed than that of the SW models.

The effects of spine-to-moment frame stiffness ratio, $K_s/K_f$, and damper-to-moment frame stiffness ratio, $K_d/K_f$, on the seismic response of the 5-, 10-, 20-, and 30-story Cnt models were studied based on the time-history analysis. Figure 15 shows the average results obtained from five ground motion inputs. As shown in Figure 15a, the maximum SDR decreases as $K_s/K_f$ increases, and tends to be constant after $K_s/K_f$ exceeds 1.0. The base shear of the 5-story model is relatively independent of $K_s/K_f$, and the base shear of the 10-story model increases until $K_s/K_f$ reaches 1.0, while the base shear of the 20- and 30-story buildings increases slowly when $K_s/K_f$ is increasing. The stiff spine frame has an effect in achieving a more uniform deformation distribution, even for structures as tall as 30 stories. Figure 15b shows that both the SDR and the base shear of the four models generally decrease when $K_d/K_f$ increases from 0 to 2.0, and then tend to be constant despite the damper stiffness. This indicates that increasing the damper stiffness is not always effective in reducing the seismic performance of the buildings.

## SEISMIC BEHAVIOR AND OPTIMAL STRUCTURAL PROPERTIES OF SGT2 MODELS

Time-history analysis with five ground motions was carried out to investigate the seismic behavior and optimal structural properties of the Sgt models. Figure 16 illustrates the

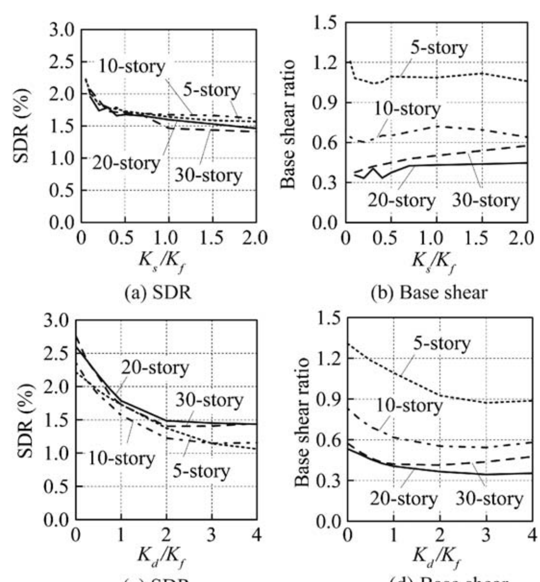


**Figure 15.** Seismic performance of Cnt models with various heights: (a) Effect of $K_s/K_f$ on SDR; (b) effect of $K_s/K_f$ on base shear; (c) effect of $K_d/K_f$ on SDR; and (d) effect of $K_s/K_f$ on base shear.

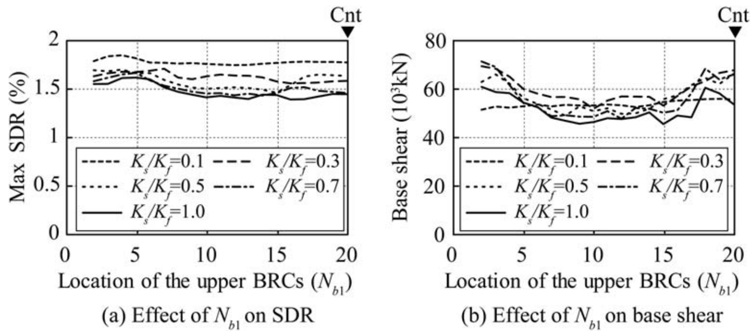


**Figure 16.** Effect of $K_s/K_f$ and $N_{b1}$ on seismic performance of Sgt2 models (model: 20-story Sgt2-Ksf0.3-Kdf1.0-1.0; input: BCJ-L2).

maximum SDR and base shear of a typical 20-story Sgt2 model, obtained by a time-history analysis with the BCJ-L2 input. The story number of the bottom spine, $N_{b1}$, ranges from 2 to 19; $K_s/K_f$ varies among 0.1, 0.3, 0.5, 0.7, and 1.0. Both $K_{d1}/K_f$ and $K_{d2}/K_f$ are kept constant at 1.0. When $K_s/K_f$ is 0.1, the curves of SDR and base shear are almost flat, indicating that the spine frame is too soft to reduce the response of the moment frame. When $K_s/K_f$ is not less than 0.3, the maximum SDRs of the Sgt2 models achieve the smallest values when $N_{b1}$ is around 10–15, but are still similar to those of the Cnt models, as shown in Figure 16a. From Figure 16b we see that the base shear of the whole structure reaches the smallest value when $N_{b1}$ is around 10–15. As for the Sgt2 models with various $K_s/K_f$ and $K_d/K_f$, the optimal configurations can have $N_{b1}$ range from 10 to 15.

As two examples among the optimal cases, Models Sgt2-Ksf0.3-Nb10 and Sgt2-Ksf0.3-Nb15 were used to search the optimal damper stiffness of the upper spine frame. Figure 17b and 17d show the average results for maximum SDR and base shear of the Sgt2 and Cnt models obtained from the time-history analysis.

Generally, in the 0.5–1.0 range of $K_{d1}/K_f$, the SDR of the Sgt2 model is less than that of the Cnt model, and the base shear is reduced by almost 25% in the Sgt2 model. The effect when $K_{d2}/K_{d1}$ (defined as $R_{Kd}$) is varied among 0.5, 0.75, and 1.0 was also studied. However, the effect of $R_{Kd}$ on the SDR is negligible in both models. Similar results have been observed for the base shear when $K_{d1}/K_f$ is less than 1.0. When $K_{d1}/K_f$ is larger than 1.0, a $R_{Kd}$ of 0.5 gives the smallest base shear. Figure 17a and 17c show the SDR and story shear distribution of two Sgt2 models, Sgt2-Ksf0.3-Nb10-Kdf1.0-0.5 and Sgt2-Ksf0.3-Nb15-Kdf1.0-0.5, along with the Cnt-Ksf0.3-Kdf1.0 model. We observe a more uniformly distributed SDR and linearly distributed story shear in the Sgt2 models. Moreover, both the maximum SDR and the base shear of the Sgt2 models are reduced compared to those of the Cnt model. The Sgt2 and Cnt models possessing dampers of the same total size were also examined. The Sgt2-Ksf0.3-Nb10-Kdf0.5-0.5, Sgt2-Ksf0.3-Nb15-Kdf0.5-0.5, and Cnt-Ksf0.3-Kdf1.0 models were compared, and the results showed that the base shear force could be reduced by adopting the Sgt2 models.

The effects of $K_{d1}/K_f$ and $R_{kd}$ in the 30-story models were also investigated, as shown in Figure 18a–18d. The effects of $N_{b1}$ in the 30-story models are almost the same as those in the

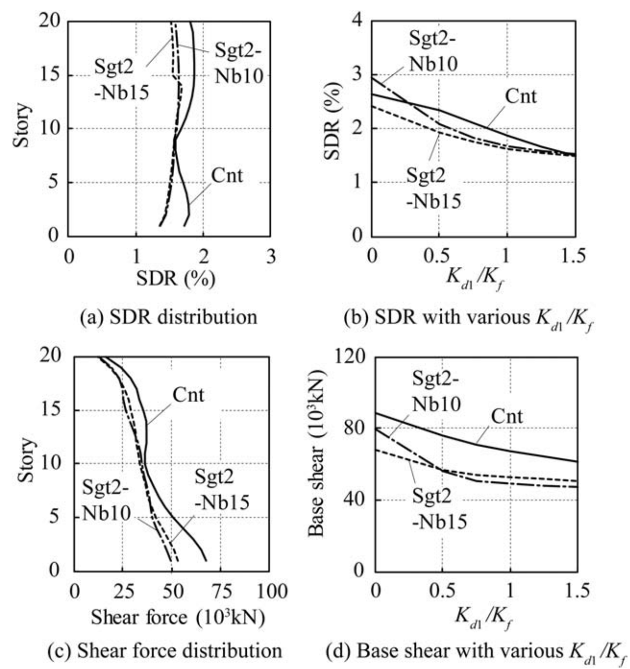


**Figure 17.** Comparison of 20-story Cnt and Sgt2 models ($K_s/K_f = 0.3$ and $K_{d2}/K_{d1} = 0.5$ in Figure 17a–17d; $K_{d1}/K_f = 1.0$ in Figure 17a and 17c; average results).

20-story models. The optimal value of $N_{b1}$ is around 15–23, 50%–75% of the total height, in which both the SDR and base shear achieve the smallest response.

## SEISMIC BEHAVIOR AND OPTIMAL STRUCTURAL PROPERTIES OF SGT3 MODELS

Three-segment spine (Sgt3) models were also tried for the 30-story building. Time-history analyses of the Sgt3 models with different segmentations were carried out. In those models, $N_{b1}$ ranges from 10 to 20 and $N_{b2}$ ranges from ($N_{b1}$ + 4) to 28, and $K_s/K_f = 0.3$, $K_{d1}/K_f = K_{d2}/K_f = K_{d3}/K_f = 1.0$. The results of the analyses show that the different configurations of those Sgt3 models do not substantially change the SDR response, as shown in Figure 19.

To compare the Sgt3 models with the Sgt2 models, for each $N_{b1}$ of the Sgt3 models we selected the cases in which the SDR was the smallest among different $N_{b2}$. The results are shown in Figure 20a and 20b. The difference in both the SDR and the base shear results between the Sgt2 and Sgt3 models of the 30-story building is negligible. This is because the BRCs of the top spine (BRC3) do not significantly work, which is indicated by the small ductility ratio shown in Figure 20c. Therefore, the 3-segment spine structure is not effective and not recommended for high-rise buildings of less than 30 stories.

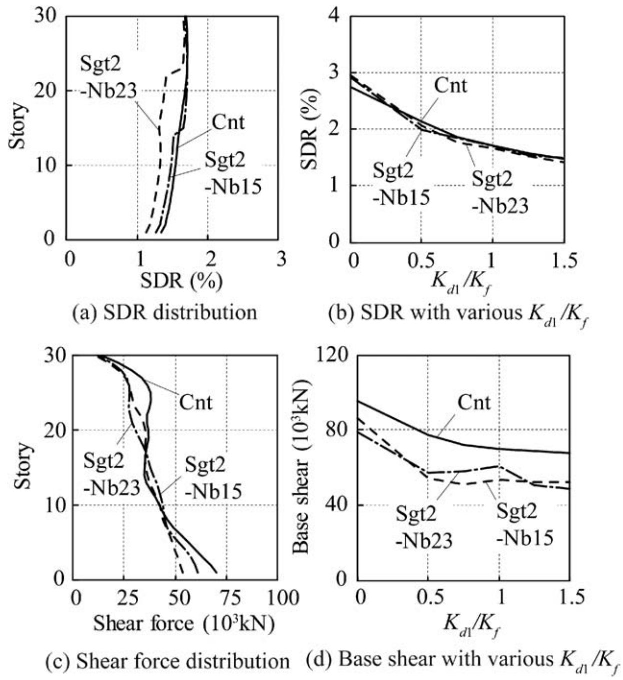


**Figure 18.** Comparison of 30-story Cnt and Sgt2 models ($K_s/K_f = 0.3$ and $K_{d2}/K_{d1} = 0.5$ in Figure 18a–18d; $K_{d1}/K_f = 1.0$ in Figure 18a and 18c; average results).

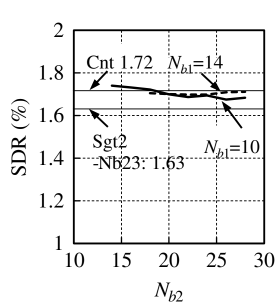


**Figure 19.** SDR of Sgt3 models with various $N_{b1}$ and $N_{b2}$ (input: BCJ-L2).

## VERIFICATION OF THE PROPOSED EVALUATION METHODS

In the following, validation of the proposed response evaluation methods is discussed. Displacement and force distribution of each component of the Cnt and Sgt2 models evaluated by MPA was compared with the results obtained from time-history analysis (THA). As shown in Figure 21, the responses estimated using MPA considering three modes agreed well with the results of the time-history analysis. From the estimated modal response,

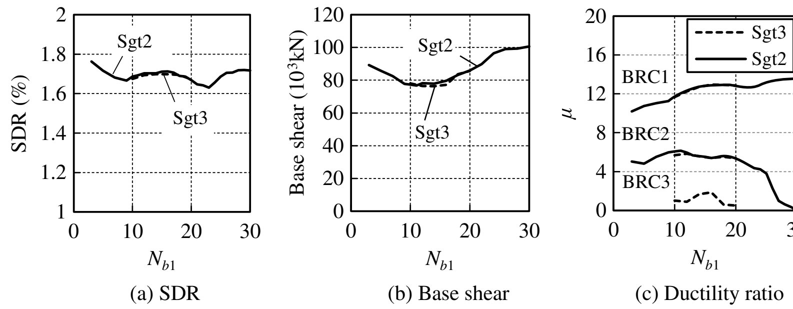


**Figure 20.** Comparison of Sgt2 model and optimal Sgt3 models (input: BCJ-L2).

we could understand that the first three modes provide enough accuracy for evaluating the seismic performance of both the Cnt and Sgt2 models. Also, the first-mode response is dominate in floor displacement, story drift ratio, shear force, and overturning moment of the moment frames. The second mode contributed to a significant response in story shear and bending moment of the spine frames (Figure 21g). The responses subjected to other input waves gave similar results.

The MPA results including the first three modes of the Sgt2 and Cnt models show that the force of the spine frames was significantly reduced in the Sgt2 models, whereas the force of the moment frames remained at a similar level compared to those of the Cnt models (Figure 21e and 21f versus Figure 21b and 21c. Meanwhile, increased moment demand for the moment frames and shear force demand for both moment and spine frames, at approximately the BRC2s level, are required (Figure 21b, 21c, and 21e).

Displacement and force distribution of each component of the Cnt and Sgt2 models evaluated by RSA were compared with the results obtained from time-history analysis. As shown in Figure 22, RSA considering three modes gives a good estimation of the deformation responses of both the Cnt and Sgt2 models. The two-stage–shaped SDR distribution is well captured in the Sgt2 model (Figure 22a) because the deformation shape is assumed to be proportional to the mode shape of the main frame, excluding the dampers. In contrast to MPA, RSA gives a slightly conservative estimate of the forces in the spine frames.

Figure 23 compares the seismic response of the Cnt models evaluated by RSA and MPA to the THA along the $K_s/K_f$ and $K_d/K_f$ indexes. Both RSA and MPA provide a good estimation with appropriate conservatism on the maximum SDR, roof displacement, shear force, and overturning moment of the moment frames of the Cnt models when $K_s/K_f = 0.1 - 2.0$ and $K_d/K_f = 0 - 1.0$. However, the error of the forces in the moment frame increased when $K_d/K_f$ increased, particularly when $K_d/K_f \geq 2.0$, as shown in Figure 23b-3 and 23b-5. The main source of error in MPA was the reference floor. Choosing a more representative reference floor, rather than the most conservative one, could greatly improve accuracy. The main source of error in RSA could be the post-yield response distribution. When the input earthquake intensity increased (and the plasticity of the structure further developed), the difference between RSA and THA decreased. Therefore, RSA provides better estimation for structures

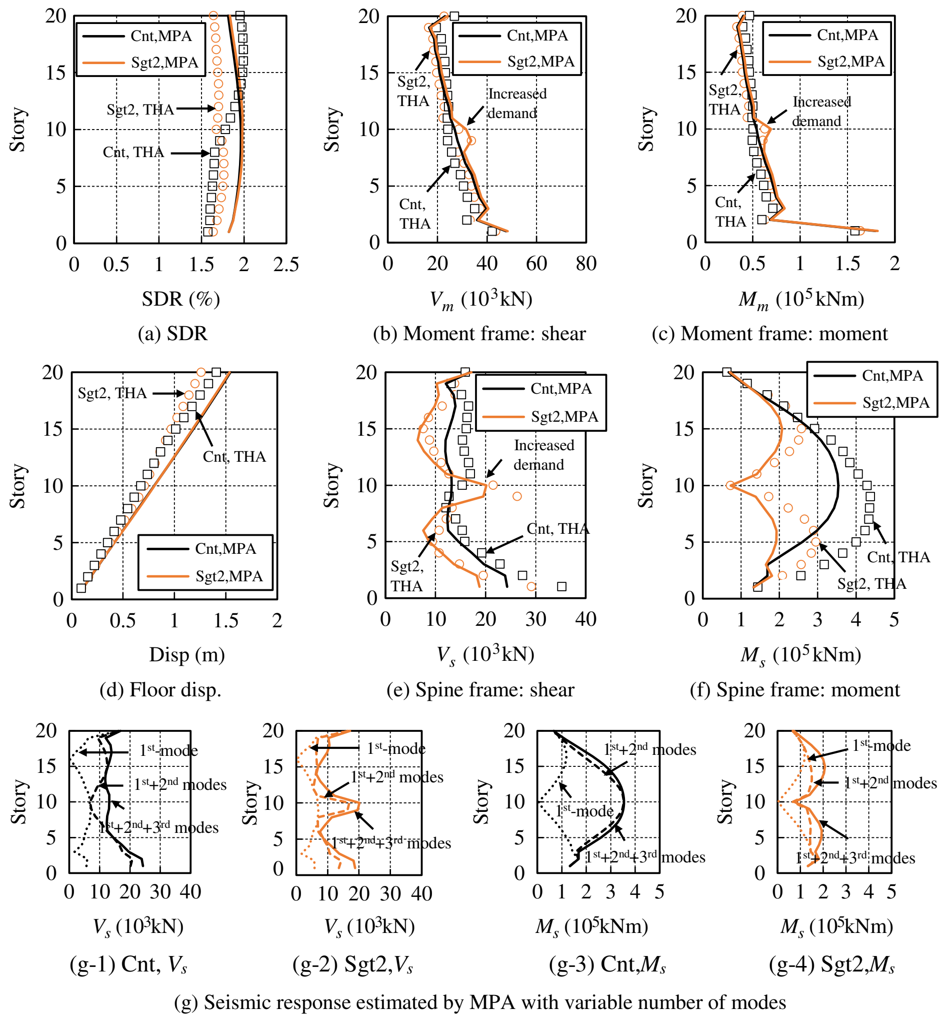


**Figure 21.** Seismic response of a Cnt and a Sgt2 model estimated by MPA and THA (models: 20-story Cnt-Ksf0.3-Kdf1.0 and 20-story Sgt2-Ksf0.3-Kdf1.0-0.5; input: BCJ-L2).

developing into sufficient plasticity or structures in which the response distribution did not change much after formation of the yielding mechanism. These results also indicate that the dampers could decrease the peak force response not only by introducing additional damping but also by changing the distribution pattern of the spine frame structures.

To modify this error, a modification factor, γ (Equation 17) is introduced for the estimation of forces of the moment frames in RSA. Figure 23b-3 and 23b-5 show the modified estimation results.

$$\gamma = 1 - 0.15K_d/K_f \tag{17}$$

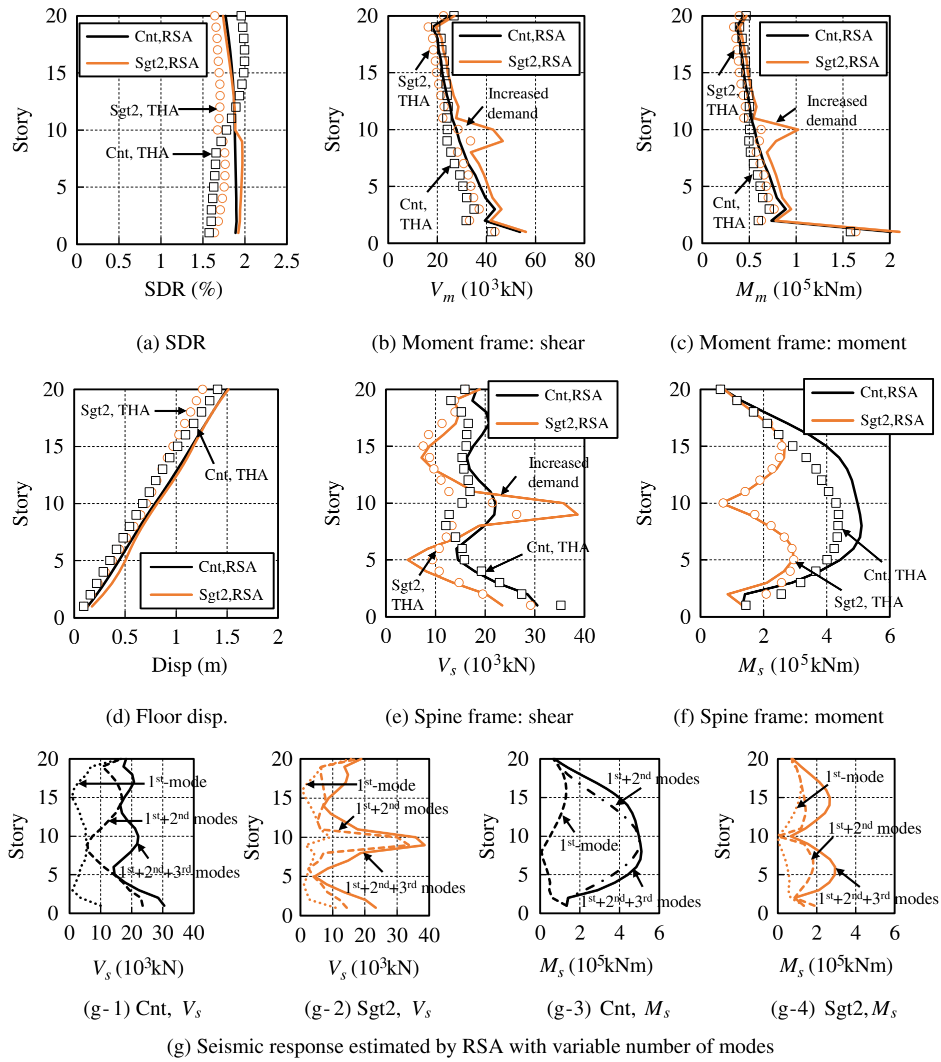


**Figure 22.** Seismic response of a Cnt and a Sgt2 model estimated by RSA and THA (models: 20-story Cnt-Ksf0.3-Kdf1.0 and 20-story Sgt2-Ksf0.3-Kdf1.0-0.5; input: BCJ-L2).

As for the Sgt2 models, RSA provided a relatively more conservative estimate of both deformation and force compared to MPA (Figure 24). Despite the values of $K_s/K_f$ and $K_{d1}/K_f$, RSA and MPA estimated the maximum SDR and roof displacement well, with proper conservatism. As for the force responses, RSA provided a better estimate for spine frames compared to MPA, particularly when $K_{d1}/K_f \leq 2.0$. Nevertheless, as with the Cnt models, the modification factor defined for the forces of moment frame of the Cnt models was also used for those of the Sgt models and gave good accuracy.

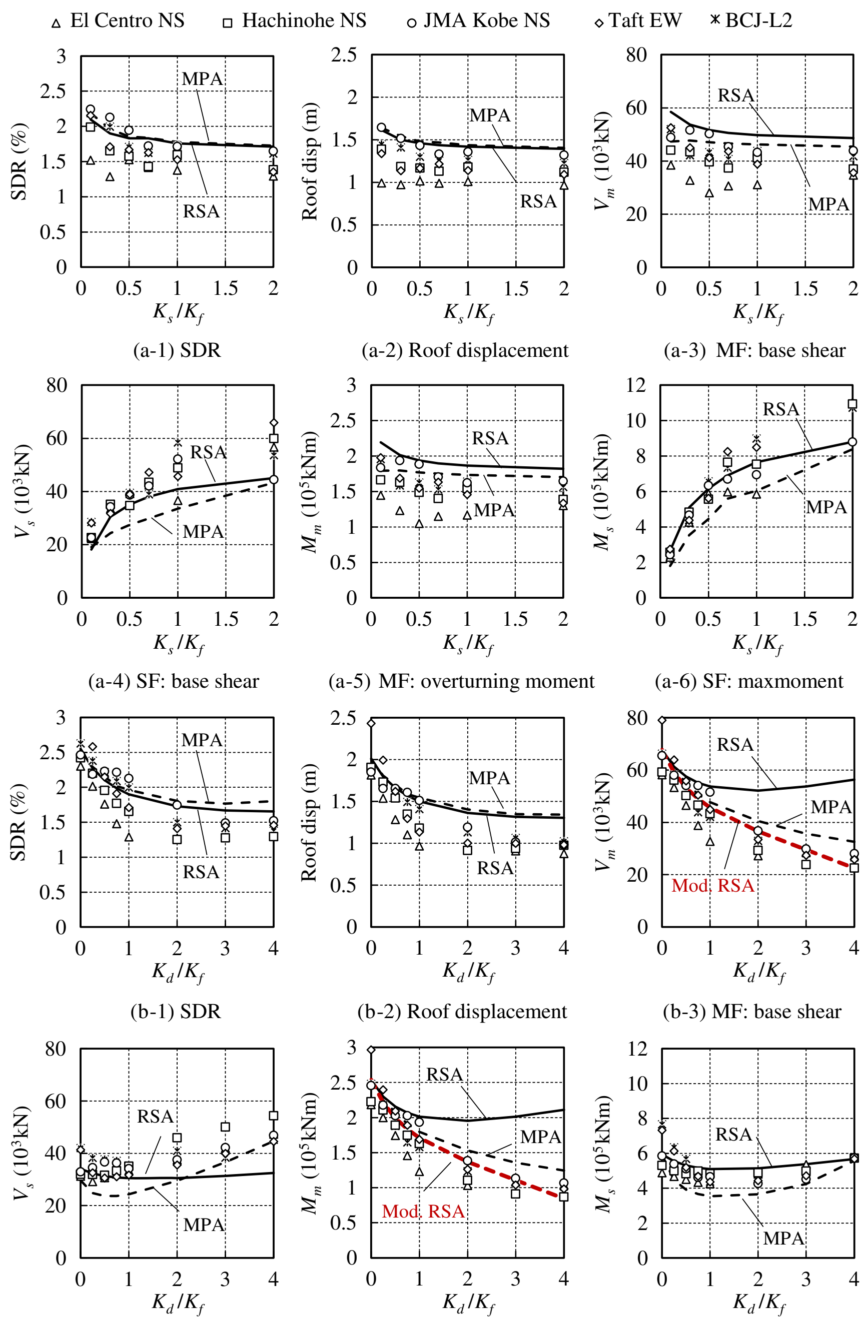


**Figure 23.** Comparison of RSA, MPA, and THA on seismic response of Cnt models: (a) with various $K_s/K_f(K_d/K_f = 1.0)$; (b) with various $K_d/K_f(K_s/K_f = 0.3)$.

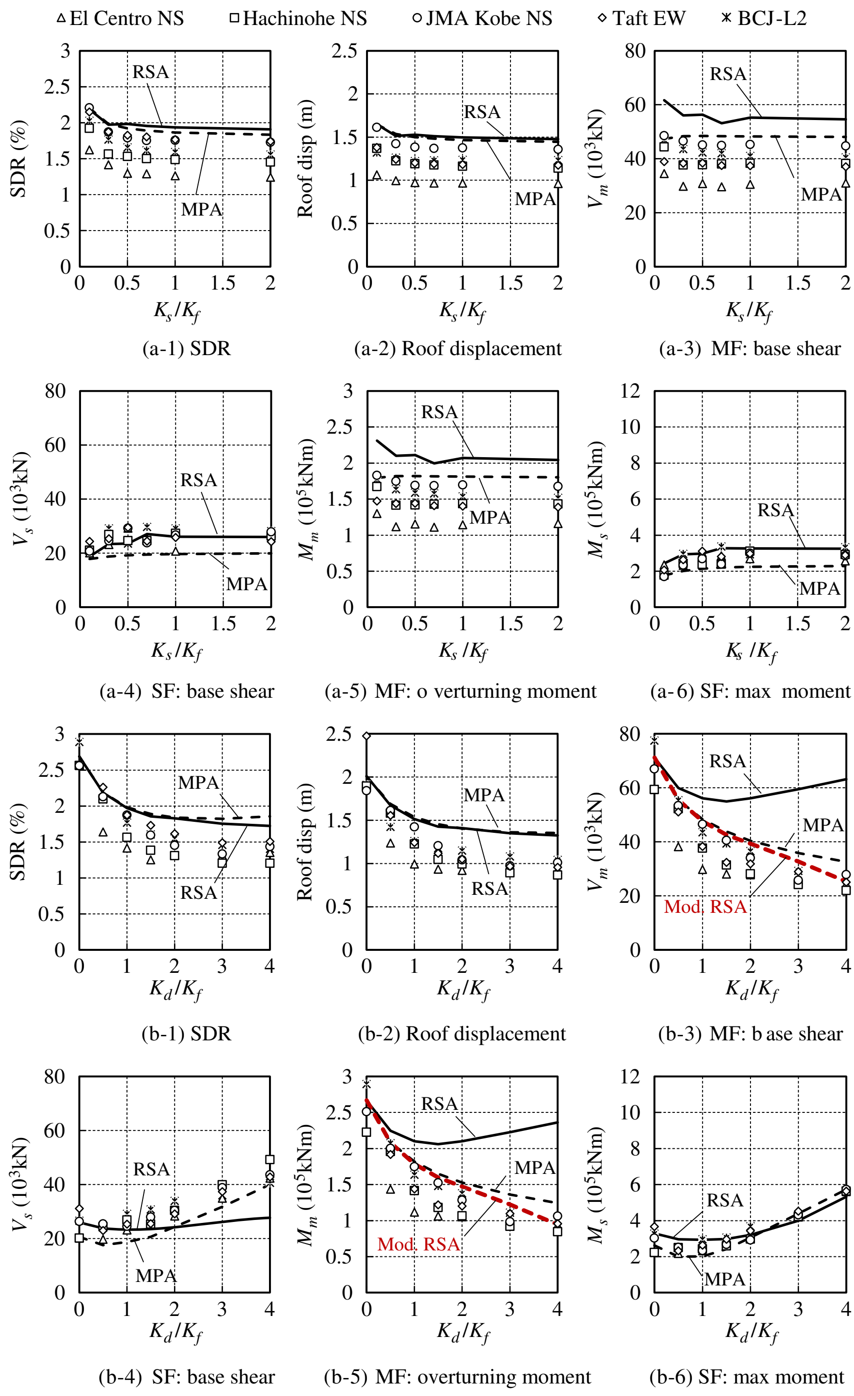


**Figure 24.** Comparison of RSA, MPA, and THA on seismic response of Sgt2 models: (a) with various $K_s/K_f(K_d/K_f = 1.0)$; (b) with various $K_d/K_f(K_s/K_f = 0.3)$.

## CONCLUSIONS

In this study, the seismic performance of high-rise buildings adopting controlled spine frame structures was studied and a segmented-spine frame configuration was proposed. Seismic evaluation methods based on modal pushover analysis and response spectrum analyses have been developed for high-rise buildings adopting continuous or segmented spine frames. A parametric study was conducted to examine the optimal ranges for key structural parameters and to verify the proposed evaluation methods. The following conclusions were drawn from this study:

- The stiff spine frame has an effect in achieving a more uniform deformation distribution, even for structures as tall as 30 stories. To ensure the effectiveness of the spine frame and dampers, the spine-to-moment frame stiffness ratio, $K_s/K_f$, should exceed 0.3 for buildings higher than 10 stories. Besides, increasing the damper stiffness is not always effective in reducing seismic performance. It is recommended that the damper-to-moment frame stiffness ratio, $K_d/K_f$, be set at up to 2.0 for the typical case of $0.3 \le K_s/K_f \le 2.0$.
- For buildings higher than 20 stories, as long as segment location $N_{b1}/N = 0.5 - 0.75$ and upper-to-lower damper stiffness ratio $K_{d2}/K_{d1} \ge 0.5$, the 2-segment spine frame model ensures a similar SDR response and efficiently reduces the base shear, compared to the continuous single-spine frame model. Therefore, the 2-segment spine frame configuration is recommended for high-rise buildings when the number of BRCs at one story is limited. The 3-segment spine frame model cannot achieve better performance than the 2-segment spine frame models, and its use is not recommended for buildings lower than 30 stories.
- The proposed MPA and RSA evaluation procedures provide good estimation with appropriate conservatism for the maximum deformation of continuous and segmented spine frame structures when $K_s/K_f \le 2.0$ and $K_{d1}/K_f \le 2.0$. Modal analysis also helps to build a deeper understanding of the dynamic response of the controlled spine frame system. The force of the moment frames, estimated by MPA, agrees well with THA results despite damper stiffness (i.e., number of dampers). However, MPA tends to underestimate the force of the spine frame. RSA improves the results compared to MPA, particularly for the maximum bending moment of the spine frame, but an additional modification factor is necessary for estimating the force of the moment frames.

## ACKNOWLEDGMENTS

This research was supported by JSPS KAKENHI (Grant No. 16J04449).

## ABBREVIATIONS

SDR: Story drift ratio
Cnt: Continuous spine frame system
Sgt: Segmented spine frame system
Prt: Partial spine frame system
SW: Shear wall system

## APPENDIXES

Please refer to the online version of this paper to access the supplementary material provided in Appendixes A and B.

## REFERENCES

Akiyama, H., and Takahashi, M., 1984. Ds-value for damage-dispersing type multi-story frames, *Journal of Structural and Construction Engineering* **341**, 54–61 (in Japanese).

Alavi, B., and Krawinkler, H., 2004. Strengthening of moment-resisting frame structures against near-fault ground motion effects, *Earthquake Engineering and Structural Dynamics* **33**, 707–722, available at https://doi.org/10.1002/eqe.370.

Chen, X., Takeuchi, T., and Matsui, R., 2017. Simplified design procedure for controlled spine frames with energy-dissipating members, *Journal of Structural and Construction Engineering* **135**, 242–252, available at http://dx.doi.org/10.1016/j.jcsr.2017.04.017.

Chopra, A. K., and Goel, R. K., 2002. A modal pushover analysis procedure for estimating seismic demands for buildings, *Earthquake Engineering and Structural Dynamics* **31**, 561–582. doi:10.1002/(ISSN)1096-9845.

Chopra, A. K., Goel, R. K., and Chintanapakdee, C., 2004. Evaluation of a modified MPA procedure assuming higher modes as elastic to estimate seismic demands, *Earthquake Spectra* **20**(3), 757–778. doi:10.1193/1.1775237.

Djojo, G. S., Clifton, G. C., and Henry, R. S., 2014. Rocking steel shear walls with energy dissipation devices, *Proceedings of the NZSEE Conference*, 21–23 March, Auckland, New Zealand.

Eatherton, M., Hajjar, J., Ma, X., Krawinkler, H., and Deierlein, G., 2010. Seismic design and behavior of steel frames with controlled rocking—Part I: Concepts and quasi-static subassembly testing, *Proceedings of the 2010 NASCC & Structures Congress*, 12–15 May 2010, Orlando, FL, 1523–1533.

Eatherton, M., Ma, X., Krawinkler, H., Mar, D., Billington, S., Hajjar, J., and Deierlein, G., 2014. Design concepts for controlled rocking of self-centering steel-braced frames, *Journal of Structural Engineering* **140**(11), 04014082.

Goel, R. K., and Chopra, A. K., 2005. Role of higher-"mode" pushover analysis in seismic analysis of buildings, *Earthquake Spectra* **21**(4), 1027–1041. doi:10.1193/1.2085189.

Janhunen, B., Tipping, S., and Wolfe, J., 2013. Seismic retrofit of a 1960s steel moment-frame high-rise using a pivoting spine, *Proceedings of the Annual Convention of the Structural Engineers Association of California*, 18–24 September, San Diego, CA, pp. 320–336.

Krawinkler, H., and Seneviratna, G. D. P. K., 1998. Pros and cons of a pushover analysis of seismic performance evaluation, *Engineering Structures* **20**(4–6), 452–464.

Lai, J., and Mahin, S., 2015. Strongback system: A way to reduce damage concentration in steel-braced frames, *Journal of Structural Engineering* **141**(9), 04014223.

MacRae, G., and Clifton, C., 2013. Rocking structure design considerations, *Proceedings of the Steel Innovations 2013 Workshop*, 21–22 February, Christchurch, New Zealand.

MacRae, G. A., Kimura, Y., and Roeder, C, 2004. Effect of column stiffness on braced frame seismic behavior, *Journal of Structural Engineering* **130**(3), 381–391.

Mazzoni, S., McKenna, F., Scott, M. H., and Fenves, G. L., 2006. *Open System for Earthquake Engineering Simulation (OpenSees)* version 2.5.0, Pacific Earthquake Engineering Research

Center (PEER), University of California, Berkeley, Berkeley, CA, available at http://opensees.berkeley.edu (last accessed May 2017).

Paulay, T., and Priestley, M. J. N, 1992. *Seismic Design of Reinforced Concrete and Masonry Buildings*, John Wiley & Sons, New York, 500–516.

Takeuchi, T., Chen, X., and Matsui, R., 2015. Seismic performance of controlled spine frames with energy-dissipating members, *Journal of Constructional Steel Research* **114**, 51–65, available at https://doi.org/10.1016/j.jcsr.2015.07.002.

Tanimura, A., and Ishida, S., 1996. Nonlinear dynamic behavior of a Shinbashira–frame system, *Journal of Structural and Construction Engineering* **42**, 635–642 (in Japanese).

(Received 8 August 2017; accepted 1 March 2018)